16 (2022) 100234

Contents lists available at ScienceDirect

International Journal of Thermofluids

journal homepage: www.sciencedirect.com/journal/international-journal-of-thermofluids

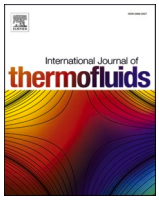

Analysis of conjugate heat transfer in a roots blower and validation with infrared thermography

Mario Matuzović [a], Sham Rane [b,*], Brijeshkumar Patel [b], Ahmed Kovačević [b], Željko Tuković [a]

[a] Faculty of Mechanical Engineering and Naval Architecture, University of Zagreb, Zagreb, Croatia
[b] City, University of London, London, United Kingdom

ARTICLE INFO

Keywords:
Conjugate heat transfer
Roots blower
Infrared thermography
Computational fluid dynamics

ABSTRACT

Oil-free Roots blower is a type of Positive Displacement Machine used for low pressure ratio applications. Its volumetric efficiency is dependent on the leakage of compressed gas through the clearance gaps. In the absence of internal cooling, prediction of temperature distribution and conjugate heat transfer becomes important for reliable design and operation. The interaction of gas flow and structural deformation in the blower is highly transient and one of the most challenging problems which need to be addressed for accurate performance prediction. To achieve this, the technique which includes moving and transforming the mesh is employed. The performance test data used for validation included discharge air temperature, mass flow rate, pressure, and power. The comparison between numerical and experimental results has shown good agreement of 7.5% on flow, 4.3% on power while the discharge temperature deviation was within 4°C. High speed infrared thermography of the rotor lobe and housing surface temperatures was used to evaluate the accuracy of the Conjugate Heat Transfer model. The difference between the experiment and simulation was within 6°C. The aim of this study was to develop and validate the numerical model for analysis of heat transfer between pressurized air and compressor elements and to provide temperature distribution in structural elements. By this means, the operational gap sizes can be reliably minimised during the design of a machine.

1. Introduction

Roots blower is a type of positive displacement machine which has a straight lobe, two lobed rotors rotate inside the casing to deliver fluid from suction to discharge, shown in Fig. 2 and Fig. 3. In current study URAI-22 oil free roots blower from Howden is considered. Oil free air from this kind of machine is used in processes of pharmaceutical, chemical, food and textile industries. One of the two rotors is described as a main rotor and another rotor is described as a gate rotor (Fig. 2), there is no contact in between the rotors and in between rotors and casing. Both the rotors are synchronized using timing gears. Gap present between two lobes is termed as interlobe clearance (Fig. 2), radial gap between rotors and casing is terms as radial clearance (Fig. 2) and gap between rotor face and casing is termed as axial clearance [1] as shown in Fig. 3. During the running condition of the machine, gas being compressed in the rotor chambers flows back into the suction chambers through these clearances, these flows are known as leakage flows. These leakage flow contributes towards degradation of the efficiency of the machine [2]. Discharge temperature of this machines increase with increase in discharge pressure. An increased discharge temperature can cause thermal expansion of the components such as rotors that move relative to the casing [3]. This leads to change in clearance size during running condition of the machine [4]. To improve the reliability of the machine, design clearance at cold conditions tend to be generally overspecified, thus loosing the potential of better efficiency. So current study focuses on the numerical and experimetal study of heat transfer from working fluid to solid components. This will help to understand the influence of leakage flow on the heat transfer, which is still not understood sufficiently for PDMs. It will also help to identify the ways to decrease the leakage losses by means of rotor tip design and reliable specification of reduced clearances.

It is difficult to get the heat transfer coefficient using simplified equation for the complex leakage flows [5]. Heat transfer in solids and fluids can be predicted and heat transfer coefficient can be derived using conjugate heat transfer analysis. Within the model, HTC can be calculated over the solid surface and it is used in structural finite element solver to calculate structural stresses and component deformation. A convection boundary condition can be replaced by direct calculations of heat transfer coefficient using CHT simulations and map solid

* Corresponding author at: SST, City University of London, 10 Northampton Square, London, EC1V 0HB, United Kingdom.
E-mail address: sham.rane@city.ac.uk (S. Rane).

https://doi.org/10.1016/j.ijft.2022.100234

Available online 19 October 2022

Nomenclature

tsf	time scale factor
Δt_f	fluid time step (s)
h	heat transfer coefficient (W m–2 K–1)
$\dot{m}$	mass flow rate (kg s-1)
Re	Reynolds number
p	pressure (Pa)
k	thermal conductivity
T_∞	free stream temperature (K)
x	length (m)
Δt_s	solid time step (s)
Nu	Nusselt number
R_s	specific gas constant (J kg–1 K–1)
T	temperature (K)
Pr	Prandtl number
ρ	density
μ	dynamic viscosity
v	specific volume (kg m–3)

Abbreviations

PDM	Positive Displacement Machine
CFD	Computational Fluid Dynamics
HTC	Heat Transfer Coefficient
PR	Pressure Ratio
CHT	Conjugate Heat Transfer
IR	Infrared
SCORG	Screw Compressor Rotor Grid Generator
IR-T	Infrared Thermography

temperatures to finite element analysis code. It is very important to define the correct boundary condition for accurate thermal analysis [6]. Clearance analysis and leakage flow CFD model of a two-lobe multi--recompression heater has been reported in [7]. Similarly, analysis of a Roots blower for Hydrogen circulating pump has been presented in [8].

Ansys Fluent was used for numerical investigation of the flow field inside the Roots blower. Mesh generated from the SCORG mesh generator is used in the study. Deforming mesh is needed to capture the highly transient nature of the flow inside the machine, for this purpose it is necessary to employ the moving mesh technique. This technique is accessible in Ansys Fluent and CFX solvers but with limited options, so a customized mesh generated in an external tool such as SCORG is needed. Kovačević [9] pioneered and implemented algebraic method to generate customized block-structured deforming mesh for twin screw rotors, which allows researchers to analyse extremely transient flow dynamics [10] in rotary positive displacement machines. The computational model for positive displacement machines such as twin-screw compressors has been described in [9] and is widely applicable, such as for the presented Roots blower model [11]. Rane [12] advanced on this technique and generated the new approach known as Rotor to Casing mesh generation method. SCORG also has other algebraic methods for mesh generation such as a two domain or a single domain topology for the two rotors [13]. The recent upgradation provides conformal mesh in a single domain for the rotor, which is employed in this research. Rane [12,13] and Kovačević [14] have presented the development and application of different types of deforming grid topologies that can be used for modelling of twin-screw machines. Applications to dry air and oil injected compressors and ORC expanders have been investigated. A bi-directional coupling of fluid flow and structural solvers was reported by Rane et al. [15]. The application was for a dry air twin-screw compressor. Conjugate heat transfer (CHT) model was used to produce boundary conditions required for the structural solver that evaluated the local leakage gap variation, in turn this was supplied to the CFD – CHT model to update the flow field. Even for the Roots blower CFD model, the deforming rotor grid is a critical element of the setup as it directly controls the interlobe and radial gap sizes. Additionally, the rotor profiles have a stepped tip design which can result into local flow features of importance. Singh et al. [10] have presented a detailed analysis of this machine while operating at low-speed conditions. PIV data of the flow in working chamber was used to evaluate the numerical model. In their study, the rotor grids that were used consisted of fixed nodes on the profile and rotating plus sliding nodes on the housing and the non-conformal interface between the two rotors, called as rotor-to-casing topology [13]. Eettisseri et al. [16] have analysed heat transfer mapping inside a reciprocating hermetic compressor by considering the rotation of crankshaft and associated motion of connecting rod and piston in a CHT model with Immersed Solid Method in the Ansys CFX solver. Dincer et al. [17] have presented a non-isothermal CFD analyses of a hermetic reciprocating compressor by means of evaluating the CHT in steady and transient models. In centrifugal compressors, CHT studies are a common design analysis practice, and several studies are available in literature [18–21]. In [18], a numerical CHT model using Ansys CFX solver was used to analyse the effect of heat transfer to the turbocharger compressor components from high temperature external heating such as the impeller shaft. Results also showed that the heat transfer through the shroud surface dominates the internal heat transfer influence on the compressor performance. An adiabatic thermal boundary was applied to the outside surfaces of the casing. Another high-pressure centrifugal compressor for a two-stage turbocharger application has been studied in [19] with CHT analysis using Ansys CFX solver. Bearing housing and turbine stage were considered as thermal boundary conditions at suitable interfaces in the model. For the experiments, temperature was measured using a telemetry system of thermocouples in the compressor wheel and on the compressor housing. However, a constant HTC was assumed for the convective boundary conditions used on the volute casing, the compressor back plate and all pipes in the model and measured temperature was used to compare results of the simulation. The effect of cooling different parts of a high-pressure centrifugal compressor has been analysed in [20] using a similar CHT model. The boundary condition applied to cooling walls was constant heat flux. Shroud, back plate and diffuser cooling were compared with respect to gain in polytropic efficiency, pressure ratio and solid impeller temperature. While in [21], the effects of heat transfer on the rotor-stator cavity temperatures were examined using adiabatic boundary condition based and CHT based model. The external surfaces of the casing were defined by natural convection correlations for HTC and ambient temperature. The adiabatic approach was found to exceed the measured cavity temperatures by 40%, whereas the CHT calculation yielded significantly better results within an error of 1 – 4%. In his PhD thesis, York [22] has studied Internally Cooled Gas Turbine Air foils at extremely high temperatures with CHT and Turbulence modelling methods using Ansys Fluent solver. To correct an excessive heat transfer being predicted on the vane suction surface, a new eddy-viscosity-based turbulence model was developed to include correct sensitivity to the effects of streamline curvature. CHT in a straight, non-rotating rib-roughened cooling channel has been studied in [23,24]. Infrared imaging was used to record surface temperature and the conduction pattern through the wall thickness was calculated by means of Ansys Fluent and COMSOL CHT models. Dittus-Boelter correlation (Eq. (1)) has been used for the specification of heat transfer coefficient at convective boundary surfaces of the channel in the CHT simulation.

$$Nu_x = \frac{\mathbf{hx}}{\mathbf{k}} = 0.023\, Re_x^{0.8} Pr^{0.4} \tag{1}$$

The study has been extended in [25], where a new CHT method is applied to solve the challenge of varying fluid and solid time scales in a rib-roughened cooling duct analysis. This method uses a weak coupling between the fluid and the solid solvers by first computing the fluid domain until it reaches a statistically steady state, from which the mean temporal solution is obtained. Then, it solves the solid domain with the mean boundary conditions imposed from the fluid generating an updated fluid boundary condition.

Analysis of a single screw compressor for thermal deformation and heat transfer has been reported in [26]. Temperature distribution on the housing was obtained by the infrared temperature camera and used as boundary condition in the numerical model using finite-element method. The authors propose that the Influence of the thermal deformation on most of the clearances could be eliminated or controlled by setting reserved clearances such as axial assembly clearance. However, the torsional deformation of the screw rotor could only be modified by compensation in machining. Correlation in Eq. (1) was used for HTC in the discharge chamber. However, in case of positive displacement machines such as twin-screw compressors or Roots blower, detailed CHT analysis are not yet available. Conventional temperature measurement technique such as use of thermocouples and RTDs are not suitable to measure entire surface temperature of the lobe during the rotating condition. Therefore, current application sought for non-intrusive experimental techniques. IR thermography has been widely used for surface temperature measurement and it provides an effective approach for non-intrusive and spatial-temporal measurement of temperature [27]. Liquid crystal thermography can also be used to measure the surface temperature, but it also required the thermochromic liquid crystal coating on the surface and imaging of change in colour of coating [28]. By considering the recent advancement in infrared thermography technique with better characteristics such as thermal resolution, pitch and dynamic range [29,30] it found to be the suitable method for this application, and it is employed to measure the surface temperature of the lobe in running condition of the machine in this study. Recent technology also facilitates the phase-locked detection of surface temperature [31] which is necessary for the current requirement of measurements. Literature also shows the use of infrared thermography to study effect of conjugate boundary condition in heat transfer analyses by investigation of local temperature measurement [32]. Significant experimental work has been carried out to understand the turbine blade tip heat transfer and aerodynamics, these studies mostly employ infrared thermography to study the heat transfer over the turbine tip surface [33] and it indicates the reliability of this technique for surface temperature measurement. IR thermography is successfully used to investigate the flows in microchannels by Liu and Pan [34], and it has been reported that IR thermography could be used to measure transient temperature along the channels.

In the numerical part of the present study, the goal was to develop a full CHT model of the Roots blower machine and use the Infrared-Thermography [35] experimental data for the validation of the modelling procedures. Such a validated CFD – CHT model could then be used to investigate in detail, the impact of heat transfer on leakage flows and thereby improve the design and performance of the machine.

2. Methodology

The goal of the numerical analysis was to develop a detailed conjugate heat transfer model of the Roots blower machine and use the Infrared-Thermography experimental data for the validation of the modelling procedures. Validation of the CFD – CHT model is required to satisfy the following quantitative data: **a.** Cycle averaged gas flow rate and the indicated power needs to be validated with the measured blower performance data, **b.** Cycle averaged gas temperature at the discharge needs to be within small deviation compared with the measured gas temperature and **c.** Quantitative surface temperature data typically obtained on the rotor lobes and the housing's external surfaces needs to be within the range of prediction obtained from thermograms. To achieve full validation, the modelling was undertaken in two stages; **I.** Axial gap calibration to tune cycle averaged flow and power and **II.** Full conjugate heat transfer model to validate rotor lobe and housing temperature. These two stages have been discussed in the following sections and in the results.

2.1. High speed infrared thermography

High speed IR thermography has been widely used for surface temperature measurement and it provides an effective approach for non-intrusive and spatial-temporal measurement of temperature. To measure temperatures accurately with IR Thermography, careful attention toward a proper choice of access window, elimination of specular reflections from channel walls, and estimation of local emissivity changes are required. Fig. 1a shows the mounting of the camera and the optical access designed on the test blower.

The principle of infrared thermography is based on the physical phenomenon that any body of a temperature above absolute zero (-273.15°C) emits electromagnetic radiation. There is correlation between the surface temperature and the intensity and spectral composition of its emitted radiation [35]. By determining its radiation intensity, the temperature of an object can thereby be determined in a non-contact way. Image IR 8300hp camera has been chosen, it has spectral range of 2 to 5.7 μm, and temperature range of -40 to 1500°C with full frame rate of 355Hz. The layout of the setup and actual setup is shown in Fig. 1b. To measure the lobe surface temperature during the running condition of the machine Phase lock is achieved by triggering the camera using the shaft encoder signal and LabView programming. The blower was connected with variable speed electric motor through pulley transmission system and can run up to 2700 rpm. To monitor and control the operating parameters of the machine, pressure and temperature sensors are installed at suction, discharge, and orifice. Shaft encoder and torque meter are used to measure the speed and power of the blower. The flow of the machine is measured using orifice. A ball valve is installed in the discharge line of the machine to regulate the discharge pressure. All sensors were connected with National instrument-based data acquisition system, and real-time data were recorded.

2.2. Axial gap calibration

The rise in temperature of rotors and casing affects internal clearances and thus it causes changes in volumetric efficiency. If compression is 100% efficient, it means that all of the air which flows into the inlet port will travel through the system and leave through the outlet port. The machines volume flow rate will be equal to the geometrical displacement of the volume entrapped between the rotors and the housing [36]. However, this is not the real case as there are internal clearances between the rotors and the casing. Air will flow from the high-pressure region to the low-pressure region causing losses. This research assumes rigid rotor and casing elements so the interlobe and the tip radial gap were maintained constant (Fig. 2). The changes in the gap size, and consequently mass flow rate, due to thermal deformations in the real machine are taken into account with the process of calibrating the axial clearance gap at both the rotor ends (Fig. 3). The axial gap is scaled at different operating conditions to account for fixed interlobe and tip gap size using an iterative process.

2.2.1. Computational domain for flow model

The dynamic mesh methodology which will be used here is the smoothing method in Ansys Fluent solver. It adjusts the mesh of a volume by deforming boundaries while keeping the topology constant, so there is no change in the number of nodes or connections between them. Mesh generation software SCORG is used for generating custom deforming meshes to overcome limitations of Fluent's smoothing algorithm which is inherently constrained by a small boundary movement in

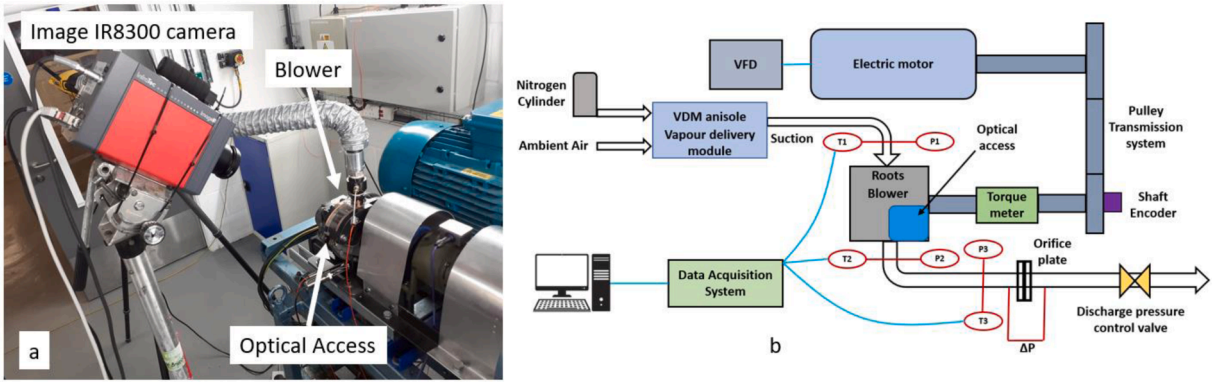

Fig. 1. (a) IR camera focused on the lobe surface, (b) Layout of the measurement system.

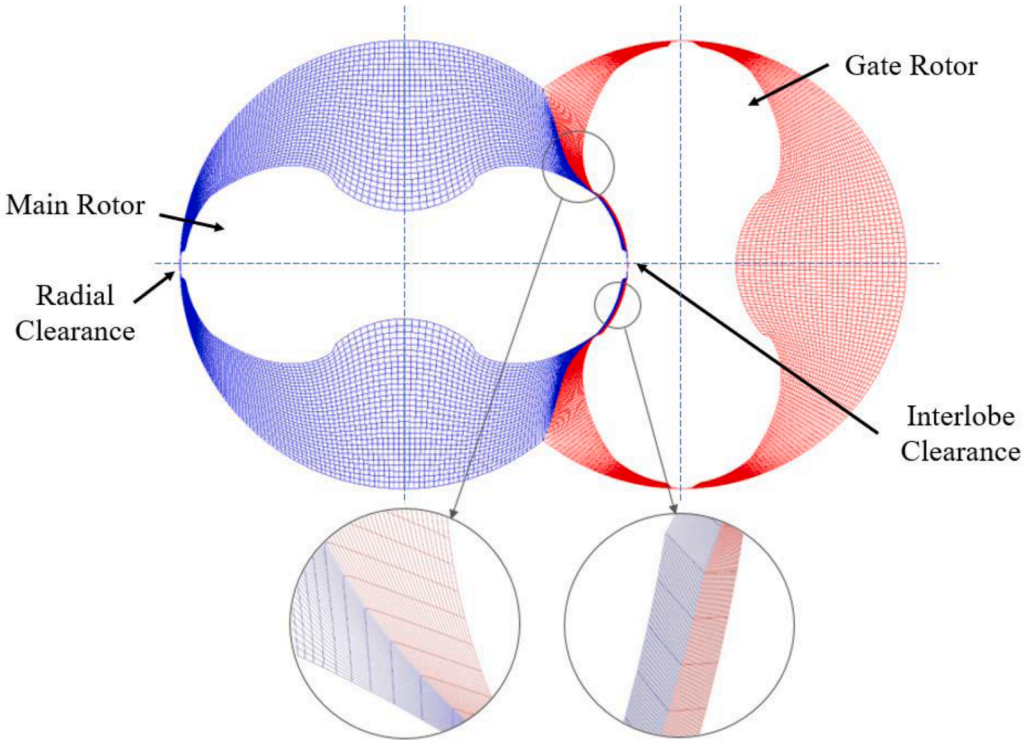

Fig. 2. Single domain Conformal mesh of the rotor generated in SCORG.

every time step. The SCORG program [13,14] generates a 2D mesh with quadrilateral cells and extrudes it to form a 3D mesh for initial rotor position. Then, it generates pre-processor input files for Fluent solver for each timestep [37]. These are text files contain information about node indices and positions. User Defined Functions developed in [37] were used to extract this information and pass it to the solver for every time step. Solver needs these input files during computations to translate the nodes. The User Defined grid deformation technique using SCORG grid and Ansys Fluent solver was experimentally validated against indicating pressure data on a rotary vane expander for ORC heat to power conversion applications in [38]. There is an option for generating a non-conformal mesh interface as well as a conformal interface. The conformal mesh shown on the Fig. 2 is generated in SCORG together with 180 pre-processor text files which contain the node positions for each angle integer. The total number of nodes in the computational domain are: 573 500. The same number of nodes are written in the pre-processor text files. The generated mesh consists of fully hexahedral cells.

From Fig. 2, every node on one side of the interface can be matched with a node on the other side so there is no interpolation necessary. This makes the calculation more accurate. Grid independency study wasn't conducted in this stage as the Axial gap size was iteratively modified to match the estimated flow and power within limits of the test data. By means of this approach, grid sensitivity was not required to be evaluated. Fig. 3 shows the composite mesh which consists of five flow domains: Inpipe, Inport, Rotor-fluid, Outport, Outpipe and Axial clearance. All these domains are fluid components and are connected via non-conformal interfaces in Fluent solver. Such an interface is fully conservative.

2.2.2. *Flow Simulation setup*

Boundary and initial conditions are applied to fully define the flow model. The operating conditions presented in Table 1 were used to specify the boundary conditions. Both, inlet and outlet boundary conditions, are defined with pressure boundary condition accordingly. The main difference in boundary conditions for different testing conditions is at the outlet which defines the static pressure value. The air temperature at the inlet was also specified as measured. Other parameters such as the

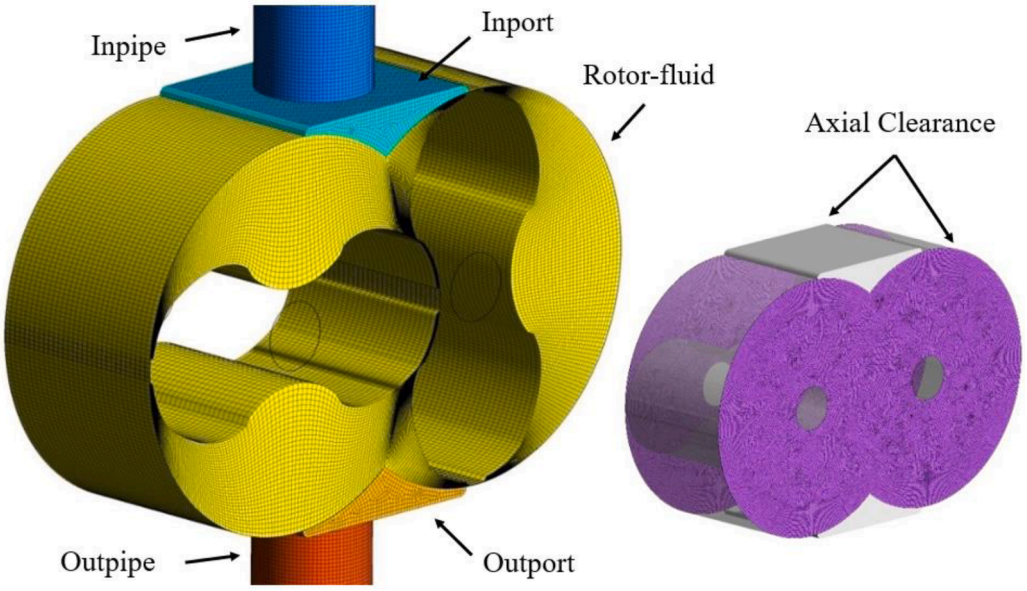

Fig. 3. Computational domain of the CFD flow model, Axial leakage gap mesh.

Table 1
Testing operating conditions.

Pressure inlet [bar]	Temperature inlet [°C]	Pressure outlet [bar]	Temperature outlet [°C]	Mass flow rate [kg/s]
1.024	29.66	1.24	52.46	0.0033
1.024	29.19	1.232	59.06	0.0063
1.023	30.03	1.23	57.72	0.0092
1.023	30.92	1.439	82.31	0.0078
1.023	33.8	1.635	139.05	0.007

turbulence intensity was set as 5% and a hydraulic diameter was assigned equal to the inpipe and outpipe diameter. The rest of boundary conditions are defined as stationary adiabatic walls with no-slip condition.

In the analysis, air has been used as a working medium and defined as an ideal gas. Flow was assumed to be subsonic [14]. Later, this assumption was confirmed to be correct by plotting the contours of Mach number in the domain of a case with highest rotational speed. Highest Mach number in the entire domain for 2000 rpm and 1.6 pressure ratio was found to be 0.4 and so the choice to go with pressure-based solver in Fluent was appropriate.

2.3. Conjugate heat transfer modelling

This section presents the methodology used for conjugate heat transfer modelling. Heat transfer to solid domains of rotors and casing is included in these calculations. First, the computational domain and case setup are presented. In the results section, the numerical solution is discussed and compared against infrared thermography data. The test Roots blower that was used to obtain empirical data was modified to include transparent sapphire glass for optical access [39]. By making the blower's rotor optically accessible, infrared thermography technique can be employed to obtain temperature fields on the surfaces [35].

2.3.1. Computational domain for CHT model

The main elements of the model are shown in Fig. 4. The blower model consists of the steel parts such as rotors and housing and the sapphire glass part which provides optical access for infrared thermography. The properties of these material are given in Table 2.

The computational mesh is made of 2 648 939 control volumes in total:

- 1 366 176 hexahedral and tetrahedral CVs in the solid domain
- 1 282 763 hexahedral CVs in the fluid domain

The geometry containing calibrated axial clearance domain (Obtained in Stage I of the analysis) and other fluid domains stayed the same. It was upgraded with the solid elements and connected by non-conformal interfaces. The computational domain thus consists of multiple subdomains connected by non-conformal boundaries. Some of the interfaces are shown in Fig. 4 along with the components of the CHT model. There are 19 non-conformal interfaces required to be defined in this setup:

- 8 fluid-fluid non-conformal interfaces
- 7 fluid-solid non-conformal interfaces
- 4 solid-solid non-conformal interfaces
- 1 fluid-fluid conformal interface between two dynamic rotor domains

All fluid-solid and solid-solid interfaces have been made using the mapped coupled wall option. The mapped mesh interface option is an alternative approach for modelling CHT between fluid-solid zones. It is more robust than the standard non-conformal interface formulations in cases where the interface zones are poorly aligned and penetrate each other or have gaps between them. Local tolerance is set to 10 in the setup. In the two solid rotor domains there is no need to control the motion of each node independently, so both rotors are specified as dynamic zones with rigid body motion. The rotational speed is applied according to the operating condition.

2.3.2. CHT simulation setup

For CHT analysis, boundary conditions were the same as in the Stage I flow analysis and can be found in Table 1. The main difference was in the specification of wall type boundaries which were not adiabatic in this model. Coupled thermal boundary condition is used at the fluid-solid and solid-solid interfaces to capture thermal interactions between these zones by enforcing continuous temperature and balance the thermal flux. This allows for obtaining the temperature field in both zones which are divided by the thermal interface. Convection thermal boundary condition is assigned on the external boundaries of the compressor. The flow field is not expected to change significantly with the inclusion of heat transfer so the numerical solution from adiabatic

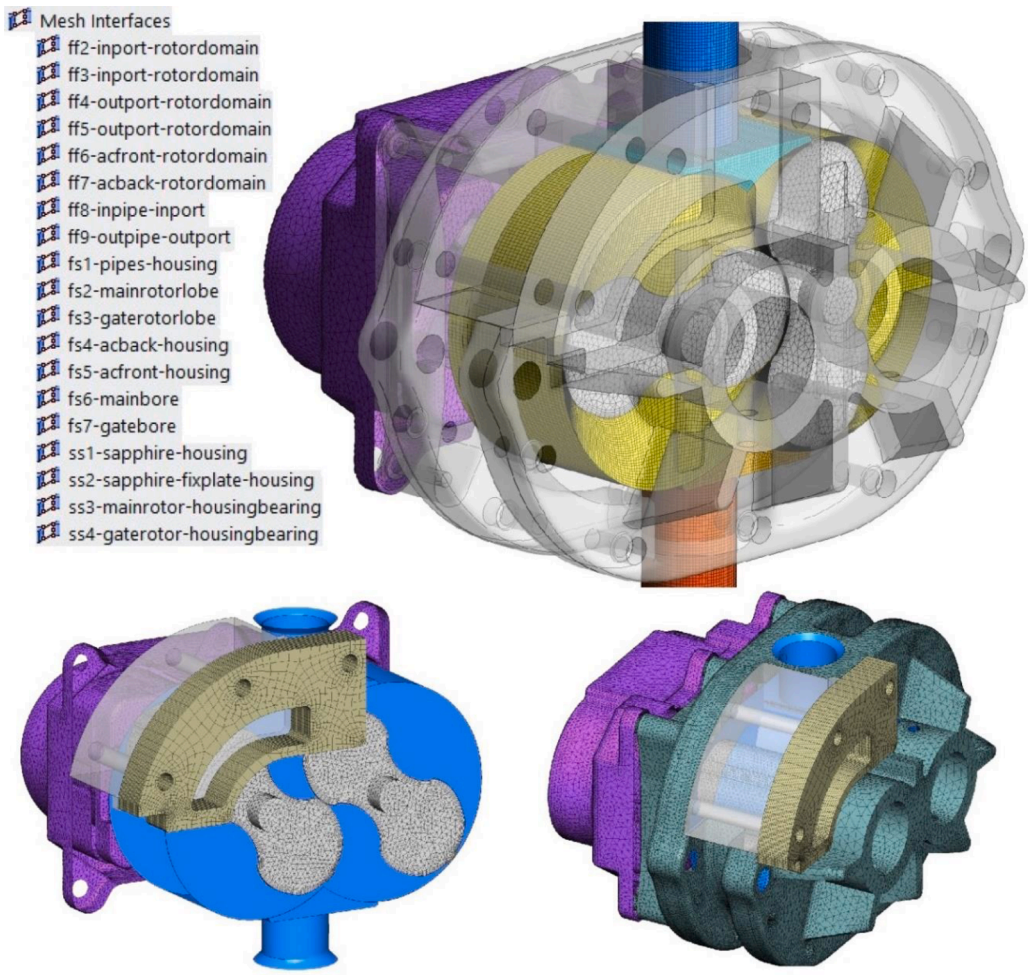

Fig. 4. Computational domain of the full CHT model.

Table 2
Material properties of glass and steel.

Property	Glass	Steel
Density [**kg/m**^{3}]	2401.7	8030
Specific heat [**J/(kgK)**]	869.99	502.48
Thermal conductivity [**W/(mK)**]	2.548	16.27

CFD simulations was used as initial condition. Fully converged solution from the non-conjugate CFD simulation is written for each case to an interpolation file and then imported to CHT case as an initial guess of the solution flow. The existing CFD model with air as the working medium was extended with solid material properties provided form Ansys Fluent material database. The following material properties of steel and sapphire glass were specified in the CHT model.

Conduction and convection processes are very different phenomena with each having its own time scale for heat transfer. This poses a problem because in the case of conjugate heat transfer, conduction represents an order of magnitude lower time scale in reaching quasi-steady state. Time marching in solid domain has to be accelerated to overcome this issue and allow for reaching quasi-steady state in reasonable amount of computational time. Fluent solver provides the option to specify an independent solid time step size which enables a different time step size to be defined for solid domain as compared to the main flow time scale. This approach was used in the current study to overcome the time scale disparity. For fluid domain, the time step is determined from the pre-defined rotational speed and crank angle step size parameter of the rotor motion. These are set in dynamic mesh of the fluid zones. The combination of these two parameters returns the time step size for the solver. Effectively, two cases with different rotational speed will return different time steps if crank angle step size and rotor grid movement per step remains the same. The ratio between the fluid and solid domain time steps can be defined as the time-scale factor *tsf* and it has been varied with the operating conditions as presented in Table 3:

$$tsf = \frac{\Delta t_s}{\Delta t_f} \tag{2}$$

Table 3
Flow data.

	1000 rpm 1.2 PR	1500 rpm 1.2 PR	2000 rpm 1.2 PR	2000 rpm 1.4 PR	2000 rpm 1.6 PR
Crank shaft speed [rpm]	1000	1500	2000	2000	2000
Crank angle step size [°]	1	1	1	1	1
Fluid zone time step [s]	0.000166	0.000111	8.33e-5	8.33e-5	8.33e-5
Solid zone time step [s]	0.833	0.833	0.833	0.833	0.833
Time-scale factor	5000	7500	10000	10000	10000

The time-scale factors are chosen to achieve the same run time for all operating conditions. This also sets the same solid zone time step size.

3. Results and discussion

The results from the Stage I – axial gap calibration study and Stage II – conjugate heat transfer analysis at five operating conditions has been discussed here.

1 1000 rpm and 1.2 pressure ratio
2 1500 rpm and 1.2 pressure ratio
3 2000 rpm and 1.2 pressure ratio
4 2000 rpm and 1.4 pressure ratio
5 2000 rpm and 1.6 pressure ratio

The selection of these operating conditions is to cover a range of low to high speed and a low to high pressure ratio.

3.1. Stage I – Axial gap calibration results

The design axial gap size of the blower was 150 um. The flow geometry and numerical grid is the same for all these cases, the only difference is in the axial gap size which is calibrated for each testing condition separately. Figs. 5-12 show the postprocessed 3D numerical results from the first gap calibration simulation at 2000 rpm and 1.6 pressure ratio. When air gets displaced through the blower, it gets compressed by the backpressure and the leakage flow from clearance gaps transfer heat to the suction air as seen in Fig. 5. As the cold low pressure incoming air gets heated by mixing with the leakage flow its density reduces and volume increases, thus decreasing the volumetric efficiency of the blower. Fig. 5 indicates that at this operating condition and with adiabatic boundary conditions to the blower surfaces, a maximum temperature of the order of 170°C is reached in the discharge pipe. Leakage from the rotor lobe tip and in the interlobe is clearly visualised.

Velocity field is presented in Fig. 6. The leakage flow is clearly visible inside the interlobe clearance gap and the two tip clearance gaps. The leakage flow is accelerated inside the gaps where it attains its maximum velocity for a given pressure difference on the two adjacent fluid chambers.

Table 4 shows the results obtained for each testing condition. The presented axial gap size value in Table 4 has been calculated using a trial-based procedure until the cycle averaged mass flow deviation with respect to measured data falls below an acceptable threshold. Mass flow rate within +/- 10% was considered acceptable.

Axial gap ranges from 143 to 250 um. This outcome is under a fixed radial and interlobe gap set in the model. Table values are total values. As there are two gaps (one at each side of the rotor), the size of each is half the total value presented in the table. The smallest gap is calculated for the highest-pressure ratio. For the same rotational velocity and higher-pressure ratios, the calibrated gap size is smaller due to larger thermal deformations which causes shrinking of the clearance gap. When the pressure ratio increases, the mass flow rate decreases. The rotor tip can be reshaped to increase leakage resistance and reduce the leakage flow through the interlobe and the tip clearance gap. The CFD models in Positive Displacement Machines are usually validated by measuring integral parameters such as the integral mass flow rate and power [36]. In the observed Roots blower, flow and power validation have been achieved in all the test cases. The largest deviation from the mass flow rate experimental result is 7.5%. Power validation has also been achieved with the largest deviation of 4.3%.

3.2. Stage II – Conjugate heat transfer analysis results

In this section, the impact of heat transfer inclusion is analysed, and numerical results are presented for measured operating conditions. In total, five different operating conditions were simulated, and the results are validated using the available experimental data obtained using high speed infrared thermography [39]. The imposed convective boundary conditions on outer walls have the same parameters h and T_∞ where, h is the heat transfer coefficient and T_∞ is the free stream temperature of air surrounding the blower. The heat transfer coefficient value of 10 W/(m^{2}K) was assigned to the outer walls of the blower, as found for turbulent isoflux plates Eq. (3) [24,40,41]. The surrounding air temperature is 25°C as measured in the test cell.

$$Nu_x = \frac{\mathbf{hx}}{\mathbf{k}} = 0.0308\ Re_x^{0.8} Pr^{1/3} \tag{3}$$

For all the simulations, iterations were performed until residuals dropped to an acceptable level of 10e-3. In Table 5, the results of CHT model are presented for each operating condition. Conduction in solid domain is accelerated by using time-scale factor to achieve compressor run time of 70 min as specified in Table 5. It can be noted that the flow validation has been preserved. Mass flow rate for each operating point matches the measurement results (Table 1). The highest achieved mass flow rate is 0.0098 kg/s, while the lowest is 0.0036 kg/s. The calculated

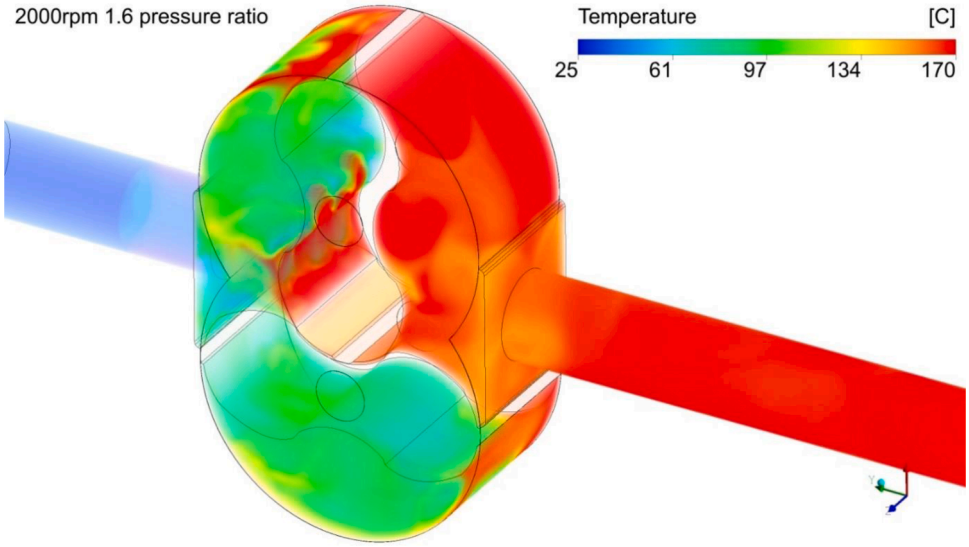

Fig. 5. Gas temperature distribution at 2000rpm, 1.6 pressure ratio.

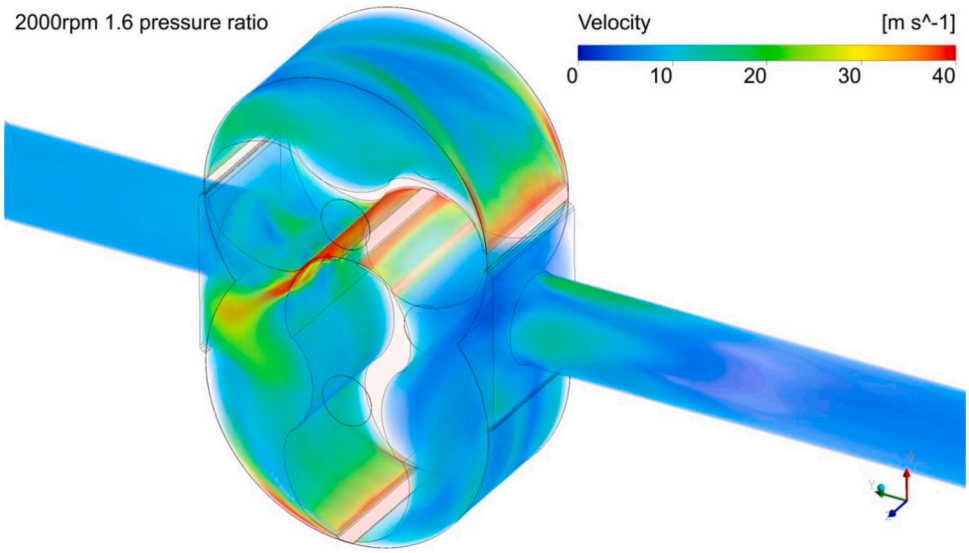

Fig. 6. Velocity distribution at 2000rpmm, 1.6 pressure ratio.

Table 4
Numerical results from non-conjugate CFD analysis.

Cases	Mass flow [kg/s]	Flow deviation %	Torque [Nm]	Power [kW]	Power deviation %	Axial gap size [um]	Exit temp. [°C]
1000 rpm 1.2 PR	0.00305	-7.53	1.56	0.16	-1.40	185	69
1500 rpm 1.2 PR	0.00614	-2.59	1.58	0.25	2.81	224	67
2000 rpm 1.2 PR	0.00947	2.97	1.62	0.34	4.27	250	66
2000 rpm 1.4 PR	0.00778	-0.25	3.14	0.66	1.78	190	105
2000 rpm 1.6 PR	0.00665	-5.04	4.57	0.96	0.72	143	168

Table 5
Conjugate heat transfer analysis results.

	1000 rpm 1.2 PR	1500 rpm 1.2 PR	2000 rpm 1.2 PR	2000 rpm 1.4 PR	2000 rpm 1.6 PR
Solid initialization temperature [°C]	37	52	52	72	117
Solid time [min]	70	70	70	70	70
Flow time [s]	0.84	0.56	0.42	0.42	0.42
Exit temperature	51	58	57	84	143
Mass flow [kg/s]	0.0036	0.0066	0.0098	0.0083	0.00735

discharge air temperatures are lower when comparing them to temperatures from the non-conjugate analysis. This is expected as heat transfers from the hot pressurized air to the rotors and casing. This heat eventually dissipates into the surrounding air. The highest discharge air temperature is 143°C, while the lowest is 51°C. A comparison with data in Table 1 indicates that the deviation is within 1 to 4°C. By calibrating the leakage gap size, the flow and power validation has already been achieved in the non-conjugate CFD model. This validation has been kept throughout the conjugate heat transfer simulation for all operating conditions. The main objective of CHT model was to validate rotor and housing surface temperatures.

The infrared thermography setup was first used to record the surface temperature data of the rotor lobes. As shown in Fig. 7a, an optical access was used, and camera was phase locked to take images at specified rotor position. These images have been used for comparison with the CHT model results in Figs. 8 to 12.

The arrangement was modified, and the infrared camera was setup to record the surface temperature of the housing as shown in Fig. 7b. In this position, a view of the low temperature at the suction, high temperature at the discharge and the temperature distribution over the housing gets captured in one view. These images were used for comparison with the CHT model results in Fig. 13.

A qualitative comparison between the numerical results obtained by CHT simulation and provided experimental data is presented here. The experimental data presented in thermograms in the Figs. 8-12 are at the surface of the male rotor for each test condition. Comparison of rotor lobe surface temperature for 1.2 pressure ratio at 1000, 1500 and 2000 rpm rotor speed are shown in Figs. 8,9 and 11 respectively. These three operating conditions are at lower pressure ratio and mostly in good agreement with experimental data. The highest deviation is seen for 1000 rpm and 1.2 pressure ratio and is around 10% with respect to the measured range (Fig. 9).

Figs. 11 and 12 show the lobe surface temperature for 1.4 and 1.6 pressure ratio at 2000 rpm rotor speed. These are the higher pressure ratio conditions, so higher temperatures are expected. Comparison with thermograms show that the transient CHT model was able to predict the results in the same range of temperature. However, it can be observed that the temperature profile on the tip is slightly different. There is a clear increase in temperature in the middle of the tip which is caused by very intense leakage flow in this area. There are also thermal traces from the axial gap leakage flow on the suction side. These are visible from both sides of the lobe. Quantitative range of the surface temperatures are well aligned with the thermograms on the right side but there is a difference in the qualitative variation of temperature field.

In Table 6, a comparison between the numerical results obtained by CHT simulation and IR Thermography data is presented for the rotor lobe regions of minimum and maximum temperatures. The general trend is that CHT model is under-estimating both minimum and maximum temperature at 1000 and 1500 rpm, 1.2 pressure ratio. While at 2000 rpm, both minimum and maximum temperatures are over-estimated by the CHT model. The highest difference between the recordings is about 5.7°C at 1000 rpm and 1.2 pressure ratio. On an

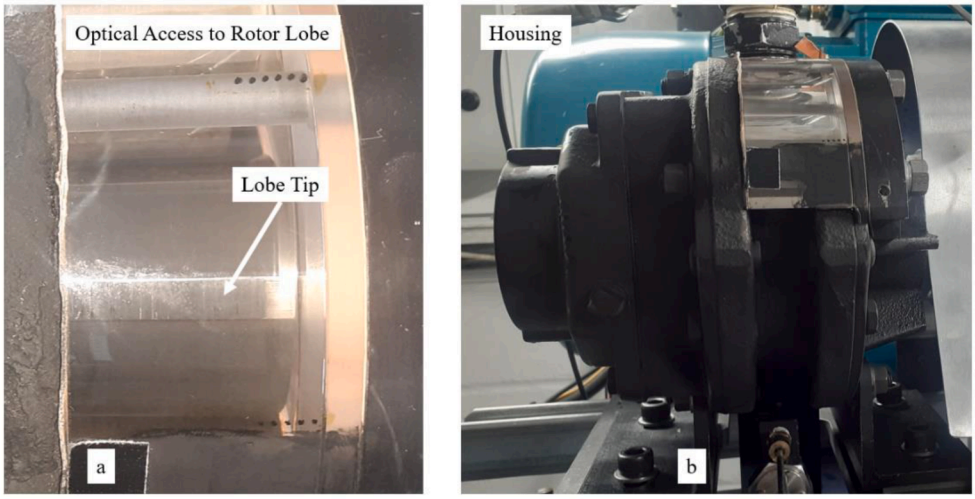

Fig. 7. Thermography camera views a) Rotor lobe surface, b) Housing surface.

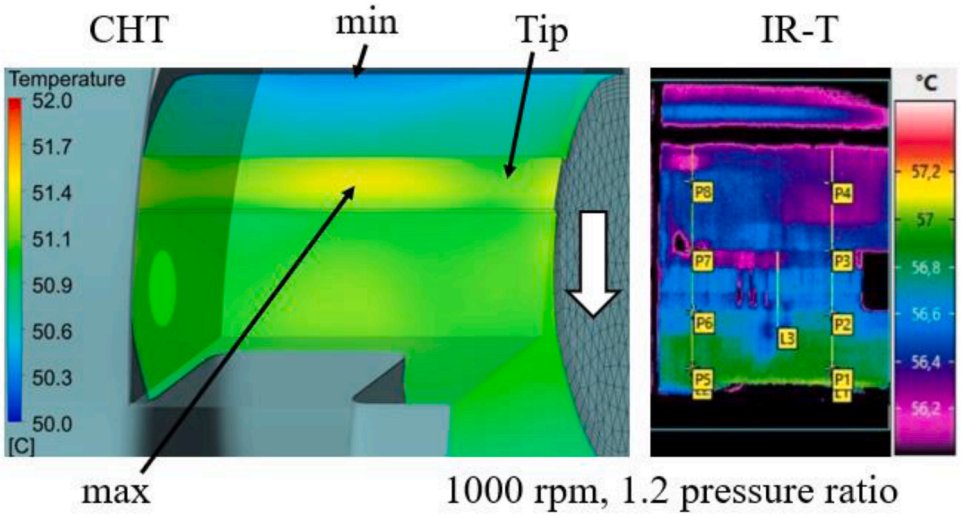

Fig. 8. Surface temperature on the rotor lobe at 1000 rpm, 1.2 pressure ratio.

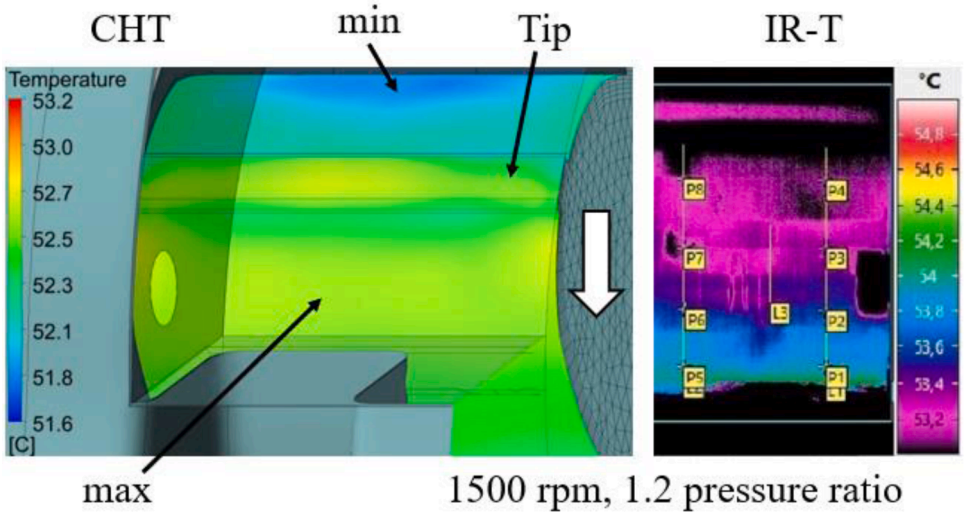

Fig. 9. Surface temperature on the rotor lobe at 1500 rpm, 1.2 pressure ratio.

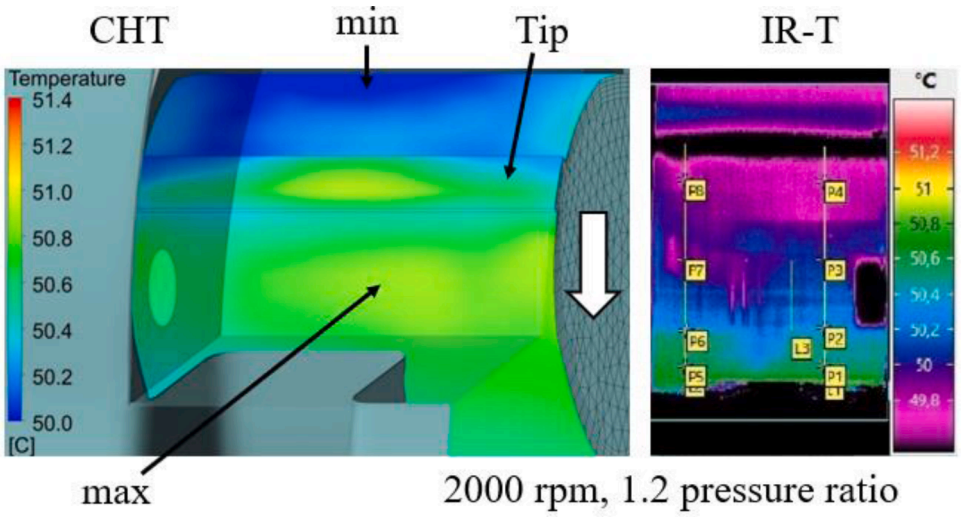

Fig. 10. Surface temperature on the rotor lobe at 2000 rpm, 1.2 pressure ratio.

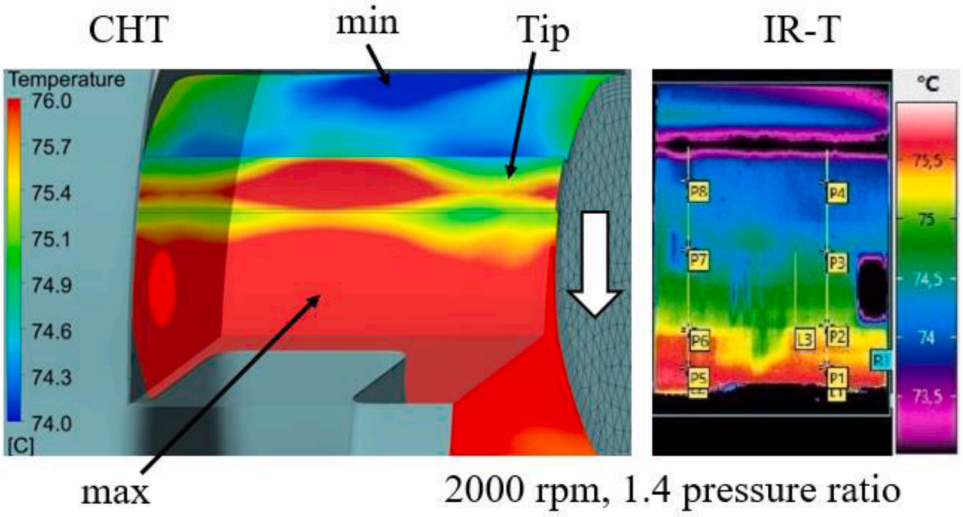

Fig. 11. Surface temperature on the rotor lobe at 2000 rpm,1.4 pressure ratio.

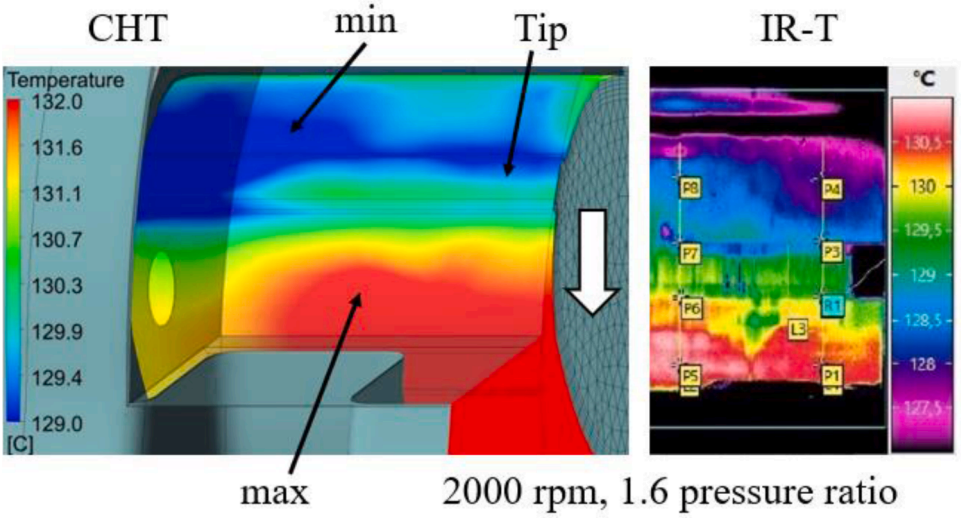

Fig. 12. Surface temperature on the rotor lobe at 2000 rpm,1.6 pressure ratio.

Table 6
Comparison of IR Thermography and CHT results on rotor lobe.

	Minimum Temperature [°C]			Maximum Temprature [°C]		
	IR-T	CHT	Difference	IR-T	CHT	Difference
1000 rpm 1.2 PR	56.4	50.3	5.7	57.2	52.0	5.2
1500 rpm 1.2 PR	53.2	51.6	1.6	54.8	53.2	1.6
2000 rpm 1.2 PR	49.8	50.0	0.2	51.2	51.4	0.2
2000 rpm 1.4 PR	73.5	74.0	0.5	75.5	76.0	0.5
2000 rpm 1.6 PR	127.5	129.0	1.5	130.5	132.0	1.5

Table 7
Comparison of IR Thermography and CHT results on housing.

	Minimum Temperature [°C]			Maximum Temprature [°C]		
	IR-T	CHT	Difference	IR-T	CHT	Difference
1000 rpm 1.2 PR	54.0	55.0	1.0	58.0	59.0	1.0
1500 rpm 1.2 PR	50.0	52.0	2.0	57.0	56.0	1.0
2000 rpm 1.2 PR	47.0	50.0	3.0	57.0	53.0	4.0
2000 rpm 1.4 PR	60.0	65.0	5.0	85.0	80.0	5.0
2000 rpm 1.6 PR	95.0	100.7	5.7	135.0	129.3	5.7

average the difference between CHT model and IR thermography temperature is about 1.85°C for the rotor lobe.

Fig. 13 presents instantaneous temperature on the exterior surfaces of the blower for the two highest pressure ratios 1.4 (Fig. 13a) and 1.6 (Fig. 13b) at 2000 rpm rotor speed. Exterior surface temperatures obtained by numerical analysis are in good agreement with infrared thermography measurements. There is a slight qualitative difference in temperature variation on the right side of the blower where the gear box is located, but it is within acceptable deviation.

In Table 7, a comparison between the numerical results obtained by CHT simulation and IR Thermography data is presented for the regions of minimum and maximum temperatures on the housing (Fig. 13). For the housing, the general trend is that CHT model is over-estimating the minimum temperature and under-estimating the maximum temperatures. The span of the temperature range is thus smaller in the CHT model data indicating more uniformity as compared to the measurement. The highest difference between the recordings is 5.7°C at 2000 rpm and 1.6 pressure ratio. On an average the difference between CHT model and IR thermography temperature is about 3.34°C for the housing which is slightly higher than that for the rotor lobe.

4. Conclusion

Conjugate Heat Transfer based CFD model has been used to analyse heat transfer from hot pressurized air to rotors, casing and surrounding components for a Roots blower application. Five operating conditions have been investigated with varying rotor speed from 1000 rpm to 2000 rpm and gas pressure ratio from 1.2 to 1.6. Simulations were carried out using Ansys Fluent CFD solver. For each operating condition, the axial clearance gap size is calibrated for validating flow and power

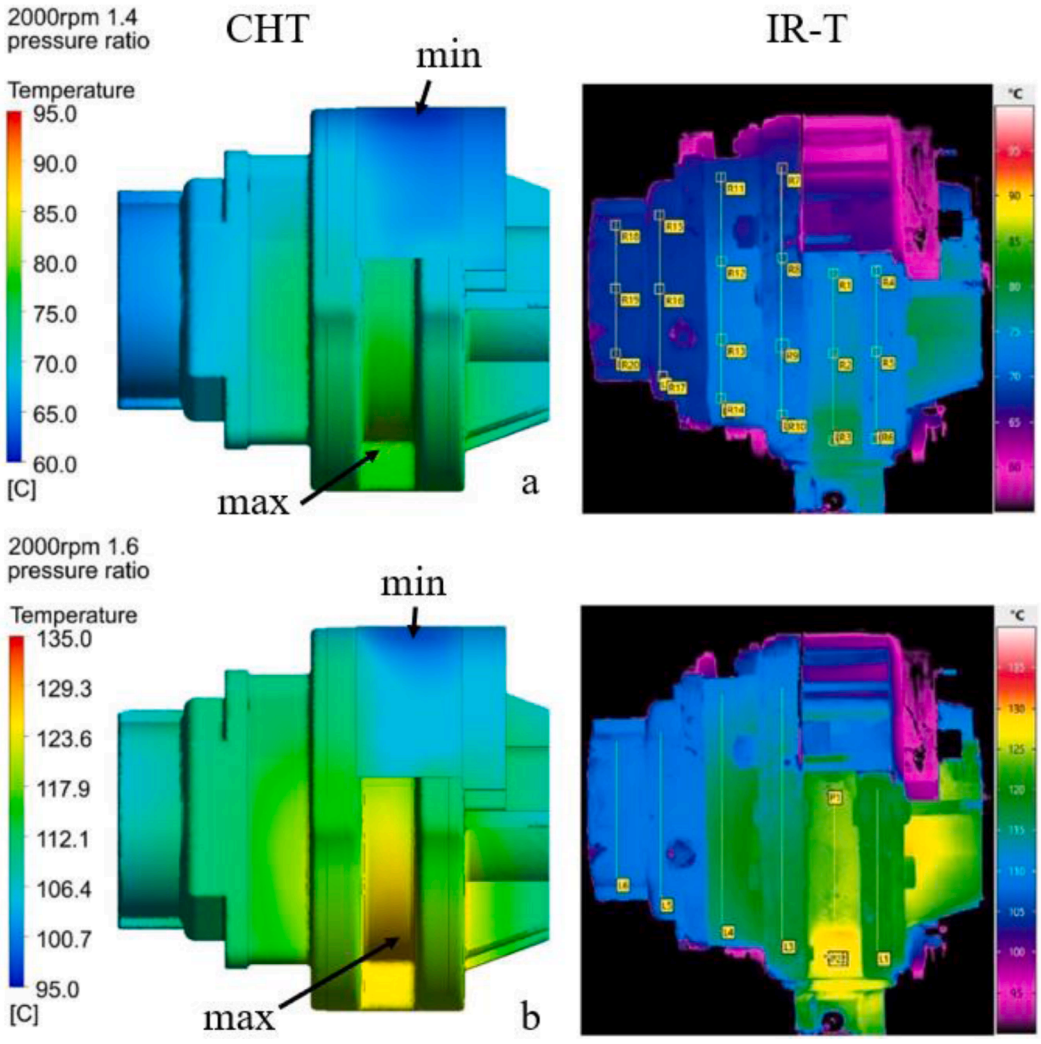

Fig. 13. Surface temperature on the blower housing at 2000 rpm, 1.4 and 1.6 pressure ratio.

predictions. The comparison with the experimental data has shown that the numerical model was able to capture the flow field adequately and provide temperature field of solid components within reasonable deviations. To achieve same power and mass flows in predictions and experiment, the axial gap size was varied from 143 to 250 um, while the radial and interlobe gap sizes were considered as constant. The following trends have been established from the analysis.

- During gap size calibration, for the rotational speed being maintained, while increasing the pressure and consequently temperature, the axial gap was decreasing. Conversely, if the same pressure ratio is maintained, while increasing the rotational speed, the axial gap was increasing as the volumetric efficiency is higher at higher speed.
- Subtle changes in size of the axial clearance gap have large impact on the mass flow rate and on the air temperature at the discharge.
- It has been observed that there are significant differences between the design clearance of 150 um and the calibrated clearance size of 70 um for 2000 rpm and 1.6 operating point. This has confirmed the assumption that there is a large room for improvement with regards to volumetric efficiency by enhancing the design of clearance gaps.
- CFD analysis which did not include heat transfer between the gas and solid elements, over-predicted the calculated exit temperature of air by up to 18°C above the measured temperature.
- By introducing convective heat transfer on the external surfaces of the blower and including conjugate heat transfer, numerically obtained and measured discharge temperatures were within 4°C.

The surface temperatures calculated using this new model are also in good agreement with the experimental data sets. However, there are noticeable differences in qualitative temperature variations at some operating conditions. The largest deviation is found to be for 1000 rpm and 1.2 pressure ratio and is around 10% with respect to the measured range of the lobe surface temperatures. This is due to a constant heat transfer coefficient that has been used in the model and this aspect needs to be improved in future studies. Furthermore, by using this knowledge the rotor tip can be redesigned. Different shapes and surface features could reduce the leakage flow and improve efficiency of the blower. The validated CHT model presented here will be used in future design modification studies.

Declaration of Competing Interest

The authors declare that they have no known competing financial interests or personal relationships that could have appeared to influence the work reported in this paper.

Data availability

No data was used for the research described in the article.

Acknowledgments

Funding for this research was received from Royal Academy of Engineering, UK, and Howden Compressors, UK, towards the project Smart Efficient Compression: Reliability & Energy Targets (SECRET).

References

[1] A. Kovacevic, N. Stosic, E. Mujic, et al., Analysis of clearances in combined screw machines, Am. Soc. Mech. Eng. Adv. Energy Syst. Div. AES 45 (2005) 35–41.
[2] J.S. Fleming, Y. Tang, The analysis of leakage in a twin screw compressor and its application to performance improvement, Proc. Inst. Mech. Eng. Part E J. Process Mech. Eng. 209 (2) (1995) 125–136.
[3] N. Stosic, On heat transfer in screw compressors, Int. J. Heat Fluid Flow 51 (2015) 285–297.
[4] D. Buckney, A. Kovacevic, N. Stosic, Consideration of Clearances in The Design of Screw Compressor Rotors, Woodhead Publishing Limited, 2011.
[5] T. L. Perelman, "On conjugate problems of heat transfer," vol. 3, no. 1, pp. 293–303, 1961.
[6] N.S. Mian, S. Fletcher, A.P. Longstaff, A. Myers, Towards obtaining robust boundary condition parameters to aid accuracy in FEA thermal error predictions, in: 2nd Annual EPSRC Manufacturing the Future Conference, 2013.
[7] A.M. Joshi, D.I. Blekhman, J.D. Felske, J.A. Lordi, J.C. Mollendorf, Clearance analysis and leakage flow CFD model of a two-lobe multi-recompression heater, Int. J. Rotating Mach. 2006 (2006) 1–10.
[8] Y. Zhang, Y. Zhao, X. Peng, Three-dimensional CFD simulation of a roots blower for the hydrogen circulating pump, Int. Compressor Eng. Conference (2018) 2625.
[9] A. Kovacevic, "Three-dimensional numerical analysis for flow prediction in positive displacement screw machines", PhD thesis, City University London, 2002.
[10] G. Singh, S. Sun, A. Kovacevic, Q. Li, C. Bruecker, Transient flow analysis in a roots blower: experimental and numerical investigations, Mech. Syst. Signal Process. 134 (2019), 106305.
[11] S. Sun, G. Singh, A. Kovacevic, C. Bruecker, Experimental and numerical investigation of tip leakage flows in a roots blower, Designs 4 (1) (2020) 3.
[12] S. Rane, "Grid generation and CFD analysis of variable geometry screw machines", PhD thesis, City University London, 2015.
[13] S. Rane, A. Kovačević, Algebraic generation of single domain computational grid for twin screw machines Part I – implementation, Adv. Eng. Software 107 (2017) 38–50.
[14] A. Kovačević, S. Rane, Algebraic generation of single domain computational grid for twin screw machines Part II – validation, Adv. Eng. Software 109 (2017) 31–43.
[15] S. Rane, A. Kovačević, N. Stošić, I. Smith, Bi-directional system coupling for conjugate heat transfer and variable leakage gap CFD analysis of twin-screw compressors, IOP Conf. Ser.: Mater. Sci. Eng. 1180 (2021), 012001, https://doi.org/10.1088/1757-899X/1180/1/012001.
[16] R. Eettisseri, M. Real, S. Oliveira, Analysis of dynamic heat transfer coefficient in a reciprocating compressor by immersed solid method in CFD, in: Int Compressor Engineering Conference, Purdue, 2021. Paper 2653.
[17] M. Dincer, K. Sarioglu, H. Gunes, A conjugate heat transfer analysis of a hermetic reciprocating compressor, 10th Int Conf on Compressors and their Systems, London. IOP Conf. Ser. Mater. Sci. Eng. 232 (2017), 012010.
[18] L. Gu, A. Zemp, R. Abhari, Numerical study of the heat transfer effect on a centrifugal compressor performance, Proc. IMechE Part C: J. Mech. Eng. Sci. (12) (2015) 2207–2220, 2015Vol229.
[19] Roclawski, H., Oberste-Brandenburg, C. & Böhle, M. (2018). Conjugate heat transfer analysis of a centrifugal compressor for turbocharger applications. 16th ISROMAC 2016. Honolulu, hal-01884259.
[20] S.M. Moosania, X. Zheng, Comparison of cooling different parts in a high pressure ratio centrifugal compressor, MDPI, Appl. Sci., 7 (2016) 16, https://doi.org/10.3390/app7010016.
[21] Stahl, M., Franz, h. Ittern, L. (2019). Conjugate heat transfer study of a centrifugal compressor with impeller cavities. global power and propulsion, Zurich. GPPS-TC-2019-0054.
[22] William York, A Robust Conjugate Heat Transfer Methodology with Novel Turbulence Modeling Applied to Internally Cooled Gas Turbine Air foils, Clemson University, USA, 2006. PhD Thesis, https://tigerprints.clemson.edu/all_dissertations/14.
[23] F Agostini, T. Arts, Conjugate heat transfer investigation of rib-roughened cooling channels, in: Proceedings of the ASME Turbo Expo 2005, USA. GT2005-68166, 2005, pp. 239–247, https://doi.org/10.1115/GT2005-68166.
[24] B Cukurel, T. Arts, Local heat transfer dependency on thermal boundary condition in ribbed cooling channel geometries, in: Proceedings of the ASME 2012 Heat Transfer Summer Conference. USA. HT2012-58519, 2012, pp. 851–862, https://doi.org/10.1115/HT2012-58519.
[25] Sebastian Scholl, Tom Verstraete, Florent Duchaine, Laurent Gicquel, 2016, Conjugate heat transfer of a rib-roughened internal turbine blade cooling channel using large eddy simulation, Int. J. Heat and Fluid Flow, Volume 61, Part B, 650-664, https://doi.org/10.1016/j.ijheatfluidflow.2016.07.009.
[26] Z. Zhang, W. Wu, Numerical investigation of thermal deformation of meshing pairs in single screw compressor, Appl. Therm. Eng. 188 (2021), 116614, https://doi.org/10.1016/j.applthermaleng.2021.116614.
[27] Vinod Narayanan. (2003). Temperature measurements and surface visualization in microchannel flows using infrared thermography. ICMM2003-1117.
[28] V.E. Srinath, H. Je-Chin, A transient liquid crystal thermography technique for gas turbine heat transfer measurements, Measurement Sci. Technol. 11 (7) (2000) 957. http://stacks.iop.org/0957-0233/11/i=7/a=312.
[29] Saux, V. Le, & Wode, S. (n.d.). Performance comparison between imageIR ® 8300 hp and imageIR ® 10300 on a thermoelastic stress analysis experiment performance comparison between imageIR ® 8300 hp and imageIR ® 10300 on a thermoelastic stress analysis experiment. 3722.
[30] O. Breitenstein, S. Sturm, Lock-in thermography for analyzing solar cells and failure analysis in other electronic components, Quantitative InfraRed Thermography J. 16 (3–4) (2019) 203–217, https://doi.org/10.1080/17686733.2018.1563349.
[31] I. Jonsson, V. Chernoray, R. Dhanasegaran, Infrared thermography investigation of heat transfer on outlet guide vanes in a turbine rear structure, Int. J. Turbomachinery, Propuls. Power 5 (3) (2020).
[32] B. Cukurel, T. Arts, C. Selcan, Conjugate heat transfer characterization in cooling channels, J. Therm. Sci. 21 (3) (2012) 286–294.
[33] Q. Zhang, L. He, Turbine blade tip aero-thermal management: some recent advances and research outlook, J. Glob. Power Propuls. Soc. 1 (1985) (2017) K7ADQC.

[34] T.L. Liu, C. Pan, Infrared thermography measurement of two-phase boiling flow heat transfer in a microchannel, Appl. Therm. Eng. 94 (2016) 568–578.
[35] J.R. Speakman, S. Ward, Infrared thermography: principles and applications, Zoology 101 (1998) 224–232.
[36] S. Mcdougald, B.W. Imrie, B.N. Cole, An investigation of the volumetric. efficiency of a roots blower, Int. Compressor Eng. Conference (1974).
[37] G Bianchi, S Rane, A Kovacevic, R Cipollone, Deforming grid generation for numerical simulations of fluid dynamics in sliding vane rotary machines, Adv. Eng. Software 112 (2017) 180–191, https://doi.org/10.1016/j.advengsoft.2017.05.010.
[38] Bianchi G, Rane S, Kovacevic A, Cipollone R, Murgia S, Contaldi G. Numerical CFD simulations on a small-scale ORC expander using a customized grid generation methodology. Energy Procedia. 2017;129:843-50. DOI:10.1016/j.egypro.2017.09.199.
[39] B Patel, A. Kovacevic, A Krupa, ''On measuring velocity and temperature in leakage flows of oil free rotary positive displacement machines'', Lecture Notes in Networks and Systems New Technologies, Development and Application IV. 2021.
[40] Y.A. Çengel, Heat Transfer: A Practical Approach, 2nd Edition, McGraw-Hill, 2002. ISBN 139780072458930.
[41] F. Mohebbi, B. Evans, Simultaneous estimation of heat flux and heat transfer coefficient in irregular geometries made of functionally graded materials. 2020, Int. J. Thermofluids 1–2 (February 2020), 100009, https://doi.org/10.1016/j.ijft.2019.100009. Volumes.